International Journal of Thermofluid Science and Technology (2023)
Volume 10, Issue 3, Paper No. 100301
https://doi.org/10.36963/IJTST.2023100301
Research Article

Finite element analysis for electro-osmotic Erying-Powell fluid flow past a stretching sheet with an exponential heat source - an ANN approach

S. Ramprasad[1], Nagabhushana Pulla[*, 2], Y. S. Kalyan Chakravarthy[1]

[1] *Dept. of Mathematics, M.S. Ramaiah Institute of Technology, Bangalore, Karnataka, India.*
[2] *Dept. of Mathematics, RV Institute of Technology & Management, Bangalore, Karnataka, India.*

ATICLE INFO

Received: 23 Mar. 2023;
Received in revised form:
21 April 2023;
Accepted: 20 June 2023;
Published online:
25 Jun. 2023

Keywords:
Electro-osmotic flow,
Erying-Powell fluid,
Exponential heat source,
FEM,
ANN.

ABSTRACT

This paper gives the numerical analysis for an electro-osmotic Eyring-Powell fluid flow that is in two dimensions along a stretched sheet. The modified governing equations are resolved by the finite element technique. Graphs are used to display the various properties for several relevant factors on dimensionless velocity and temperature fields. The results are compared with previous findings in order to confirm the accuracy of the numerical solution. There appears to be a decrease in velocity when the magnetic parameter and Eckret number increase. This study has implications for fluidization, environmental pollutants, and agriculture. In this study, computational fluid dynamics (CFD) simulations and an artificial neural network (ANN) model are both employed.

1. Introduction

The qualities of fluids that defy Newton's rule of viscosity have been the subject of research for the last few decades. The usage of these fluids becomes more appropriate than Newtonian fluids in various industrial and physiological sectors. Blood, ceramics, fruit juices, printer inks, shampoos, polymer solutions, cosmetic products, paint sand, and other substances are examples of non-Newtonian fluids. For a better understanding of the various flow behaviors of these sort of fluids, various models are available in the literature. However, researchers have shown that it can be challenging for a specific non-Newtonian model to account for all possible non-Newtonian behaviors. One of the non-Newtonian fluids is the Eyring-Powell fluid model, which was developed in 1944 by Powell and Eyring [1]. Essential applications for the Eyring-Powell fluid model can be found in a wide range of geophysical, industrial, and natural phenomena. These crucial applications include enhanced oil recovery, thermal insulation, fog formation and dispersion, orchards of fruit trees, pollution in the environment, drying of porous substances, and subsurface energy conveyance. The Eyring-Powell fluid has also drawn a lot of attention for the reasons listed below, even though its mathematical analysis is more challenging. Eyring-Powell fluid acts like a Newtonian fluid under low and high shear rates. Noreen Sher Akbar et al. [2] investigated the MHD flow of the Eyring-Powell fluid on a stretching sheet. They implemented finite difference scheme to analyse various parameters graphically. The effects of slip on the peristaltic flow with wall

[*]*Corresponding e-mail*: *nagabhushanamk.rvitm@rvei.edu.in* (Nagabhushana Pulla)

Nomenclature

a	Stretching rate	Re_x	Local Reynolds number, $Re_x = \frac{a x^2}{\upsilon}$
B_0	Magnetic field strength	T_∞	Ambient fluid temperature
B_i	Biot number, $B_i = \frac{h_s}{k}\sqrt{\frac{\upsilon}{a}}$	*Greek symbols*	
M	Magnetic parameter, $M = \frac{\sigma B_0^2}{\rho a}$	ξ	Material parameter, $\xi = \frac{1}{\rho \upsilon \beta_1 C}$
C_f	Skin friction coefficient	δ	Fluid parameter, $\delta = \frac{a^3 x^2}{2C^2 \upsilon}$
Ec	Eckert number, $Ec = \frac{a^2 x^2}{C_p (T_w - T_\infty)\upsilon}$	υ	kinematic viscosity $(\mathrm{m^2/s})$
E_1	Electric parameter, $E_1 = \frac{E_0}{a x B_0}$	μ	dynamic viscosity $(\mathrm{kg/m\,s})$
f	Dimensionless velocity of the fluid phase	ρ	density of the fluid $\left(\mathrm{kg/m^3}\right)$
Nu	Nusselt number	β_1, c	material constants
Pr	Prandtl number, $Pr = \frac{\mu Cp}{k}$	η	similarity variable
Q_e	Exponential heat source parameter, $Q_e = \frac{QE^*}{\rho C_p a}$	θ	dimensionless fluid temperature

characteristics was studied by Hina [3]. Hayat et al. [4] deliberated heat generation/absorption effects on Nanofluid flow over an impermeable stretched cylinder. They observed that high temperatures cause the radiation parameter to raise. The nanofluid across an exponentially stretched sheet is investigated by Srinivas Reddy et al. [5]. In this study it is perceived that raising the suction parameter and the material parameter, the velocity profile is reduced, but the material parameter exhibits the opposite trend. Gholinia et al. [6] examined the Eyring-Powell fluid Nano flow on a disk. Amin Jafarimoghaddam [7] deliberated the influence of thermal boundary condition on Eyring-Powel fluid flow over a sheet. Atul Kumar Roy et al. [8] illustrates Eyring-Powell fluid flow past a plate by considering convective boundary conditions. Waqas et al. [9] studied the Eyring fluid past a stretching sheet. The analysis of heat and mass transport for a viscoelastic fluid channel has been studied by Arshad Riaz [10]. The author noticed that the aspect ratio of the rectangular duct causes the velocity profile to increase. Nisar et al. [11] investigated the MHD peristaltic flow of an Eyring-Powell nanofluid. The effects of radiation and Joule heating are included during the analysis.

Electro-osmosis is widely observed in many systems such as bio membrane, fluid dialysis, porous materials, etc. The electro-osmosis- flow in a channel has been instigated by Fazle Maboob et al. [12]. They observed that the Eyring-Powell fluid parameter supports the channel's central velocity for negative electrokinetic pumping and acts in the opposite direction for positive electrokinetic pumping. Asha Shivappa and Sunitha [13] explored the fluid past a channel consists of gyrotactic microbe. The findings show that bioconvection lowers the gradient of pressure because convection instability occurs inside

the system, which results in convection pattern and lowers gradient of pressure.

Due to its numerous uses in engineering and the environment, such as metal and polymer extrusion, etc., the flow model over the stretching sheet has recently acquired great relevance in fluid dynamics. Salleh et al [14] examined the fluid of a boundary flow on stretching sheet and also considered Newtonian heating. Makinde [15] obtained a numerical solution for buoyancy driven vertical plate with a heat source. Yasir khan et al. [16] examined the flow of a fluid with thermal conductivity and viscosity on a stretching sheet. Subhas Abel et al. [17] studied the heat transfer analysis of a Maxwell fluid flow on a stretching sheet and observed that the Maxwell parameter influences the velocity and temperature profiles. Liancun Zheng et al. [18] studied the effect of velocity slip of a nanofluid on stretching sheet. Rashid et al. [19] has discussed the effects of magnetic field on flow of nanofluid on stretching sheet. Das et al. [20] investigated numerically the nanofluid flow past over a sheet with a heat source or sink. Turkyilmazoglu [21] examined the micropolar fluid flow caused by a permeable stretched sheet. Bhatti et al. [22] studied the flow of a Williamson nanofluid over a sheet. In the existence of radiation, the convective flow of a nanofluid over a stretching sheet was studied by Nayak et al. [23]. Sumit Gupta et al. [24] examined flow of a nanofluid on a sheet with the influence of thermal radiation and analysed the results graphically. They applied various perturbation techniques to study the solutions and conclude that the optimal homotopy asymptotic method is more effective, simpler and easier than other methods. With the influence of slip conditions, Umar et al. [25] discussed the importance of activation energy strength parameter on wall mass flux and mass friction field. Hayat et al.[26] carried out Darcy-Forchheimer model on nanofluid over a curved sheet. The magnetic dipole effect sheet with thermophoretic particle deposition is taken into consideration by Naveen Kumar et al. [27]. The flow equations are numerically solved by RK iterative method. They noticed that the velocity profile gets weaker as ferromagnetic interaction parameter values rise. The unsteady flow of Casson nanofluid is examined by Wasim Jamshed et al. [28] in terms of both its heat transport and entropy. They studied the effect of slip condition and solar thermal transport on Casson nanofluid flow. Warke et al. [29] considered the steady flow of micropolar fluid over a sheet. Sohail Nadeem et al. [30] analyzed the viscoelastic fluid flow through a stretching sheet which is not linearly extending is taken into account. Suction and injection cases are also covered. The effects of viscous dissipation and brownian motion with thermophoresis are taken into consideration. Dharmaiah et al. [31] applied second order velocity slip condition, Neild's condition to investigate micropolar nanofluid along a Stretching surface. Li et al. [32] implemented homotopy analysis method to investigate Carreau nanofluid along a convectively heated sheet. Saravana et al. [33] investigated numerically the behaviour of two non-Newtonian fluids over a stretching surface. Li et al. [34] succinctly explained the impact of ohmic and viscous dissipation on plate with uniform suction. Li et al. [35] analysed numerically the influence of velocity and thermal slip effects on a ternary nanofluid over stretching sheet.

Effects from an exponential heat source is used to model the flow of a micro polar nano liquid past a stretchy surface was studied by Mishra et al. [36]. Ragupathi et al. [37] considered the the Casson nanofluid flow across a sheet with exponential heat source influences. Nagi reddy et al. [38] examined the effects of heat source on convective MHD flow across an exponentially extending surface. In the presence of exponential heat source, Mohan Krishna et al. [39] instigated the MHD Carreau fluid flows on parabolic regions. The process of heat and mass transmission is examined. A problem of heat transmission in half-space under the influence of a point non stationary heat energy source was studied by Formalev et al. [40]. Ikram Ullah et al. [41] investigated the flow of a nanoliquid in a rotating system with the influence of viscosity and thermal conductivity.

With the available literature, authors came to know that no effort has been reported yet to

discuss on electro-osmotic flow of Powell fluid flow over stretching sheet with an exponential heat source and convective boundary conditions are taken into account. The authors are motivated to look at this issue by their aforementioned uses in industries, biomedicine, and studies. By employing the Galerkin finite element method, the governing equations are solved. The related ANN model has been projected, and there is thorough discussion of the attained numerical solutions. When the magnetic parameter and Eckret number rise, the velocity seems to fall. This research has applications in the fields of fluidization, environmental pollution, and agriculture.

2. Problem definition

- We investigate an Erying-Powell fluid flowing past a stretching sheet in an incompressible, two-dimensional electro-osmotic flow, as shown in Fig. 1.
- The sheet is pulled taut, allowing the fluid to flow quickly $u_w = ax$ (a is a constant).
- A Cartesian coordinate system's x-axis and y-axis are conceptualised as being parallel to and perpendicular to the stretching surface, respectively. Normally applied, a strong magnetic field B_0 is placed over the flow.

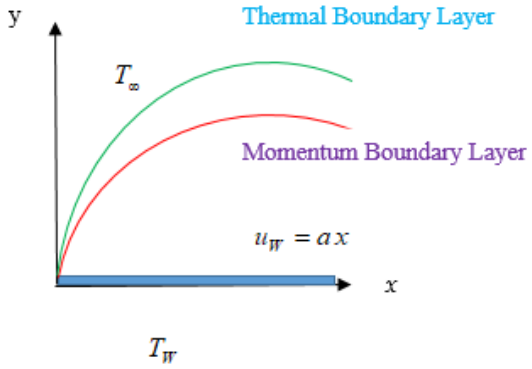

Fig.1. Physical Configuration of the Problem

- Viscous dissipation and an exponential space-related heat source are considered. The equations underlying the approximations for the boundary layer are [2, 30, 36].

2.1 Governing Equations

$$\frac{\partial u}{\partial x}+\frac{\partial v}{\partial y}=0 \tag{1}$$

$$u\frac{\partial u}{\partial x}+v\frac{\partial u}{\partial y}=\left(\upsilon+\frac{1}{\rho\beta_1 C}\right)\frac{\partial^2 u}{\partial y^2}-\frac{1}{2\rho\beta_1 C^3}\left(\frac{\partial u}{\partial y}\right)^2\frac{\partial u^2}{\partial y^2}+\frac{\sigma}{\rho}\left(E_0B_0-{B_0}^2u\right) \tag{2}$$

$$u\frac{\partial T}{\partial x}+v\frac{\partial T}{\partial y}=\frac{k}{\rho c_p}\frac{\partial^2 T}{\partial y^2}+\frac{\sigma}{\rho c_p}\left(E_0B_0-{B_0}^2u\right)^2+\frac{\mu}{\rho c_p}\left(\frac{\partial u}{\partial y}\right)^2+\frac{Q_E}{\rho c_p}(T_w-T_\infty)e^{-\sqrt{\left(\frac{b}{\upsilon_f}\right)}ny} \tag{3}$$

Conditions

$$u=u_w=ax,\ v=0,\ -k\frac{\partial T}{\partial y}=h_s\left(T-T_w\right)\ \text{at}\quad y=0 \tag{4}$$

$$u\to 0,\ T\to T_\infty\quad \text{at}\quad y\to\infty$$

Non-dimensional equations

$$(1+\xi)f'''-\xi\delta\left(f''\right)^2f'''+M\left(E_1-f'\right)-\left(f'\right)^2+f\,f''=0 \tag{5}$$

$$\theta''+Pr\,f\,\theta'+Pr\,M\,Ec\left(f'-E_1\right)^2+Pr\,Ec\left(f''\right)^2+Pr\,Q_e e^{-n\eta}=0 \tag{6}$$

Non-dimensional conditions

$$f(0)=0,\ f'(0)=1,\ \theta'(0)=-B_i\left(1-\theta(0)\right)\ \text{at}\ \eta=0 \tag{7}$$

$$f'(\eta)\to 0,\ \theta(\eta)\to 0 \text{ as } \eta\to\infty$$

2. b. Skin friction and Nusselt number

The skin friction and Nusselt number are

$$C_f = \frac{\tau_w}{\frac{1}{2}\rho u_x^2} \text{ and } Nu = \frac{x q_w}{k(T_w - T_\infty)} \text{ where } \tau_w = \left[\left(1+\frac{1}{\beta_1 c}\right)\frac{\partial u}{\partial y} - \frac{1}{6\beta_1 c^3}\left(\frac{\partial u}{\partial y}\right)^3\right] \quad (8)$$

The non-dimensional skin friction and Nusselt number are

$$c_f = \sqrt{Re}c_f = (1+\xi)f'' - \frac{\xi\delta}{3}(f'')^3 \text{ at } \eta = 0 \quad (9)$$

$$N_u = \sqrt{Re}Nu = -\theta'(0) \quad (10)$$

3. Numerical solution

Nonlinear coupled controlling equations are transformed into a matrix form by the Galerkin finite element method [42-44]. The global matrix for the entire domain is created by combining the coupled matrix equations for the individual elements, and it is then repeatedly solved to provide the velocity and temperature. To keep the findings as accurate as possible, the obtained solution's error level is set at 10^{-4}. The variance between the prior iteration and the present iteration for the variables at all nodes is reached, the iterative process comes to an end. To analyse the fluctuations in velocity and temperature, linear elements with two nodes are taken into consideration. The nodes are connected by lines to form a mesh structure. The outcomes are attained by considering 100 mesh nodes of points. To solve Equations, the Galerkin finite element method is used. (5) - (6) on a designated region $0 < \eta < 6$. By applying the Galerkin method [37], the dependent variables f' and θ are approximated by $f' = \sum_i N_i f_i', \theta = \sum_i N_i\theta_i$. For two nodes the nodal distributions can be expressed as

$f' = N_i f_i' + N_j f_j', \theta = N_i\theta_i + N_j\theta_j$, where

$N_i = \frac{\eta_j - \eta}{\eta_j - \eta_i}$ and $N_j = \frac{\eta - \eta_i}{\eta_j - \eta_i}$.

These essentials are then combined to form a global matrix with the n number of nodes. For n nodes, the element stiffness and load matrix are expressed as follows: **Table 1** Comparison of the present results with Noreen Sher et al. [2] for the skin friction in the absence of Q_e, B_i and E_1 and for $\varsigma = 0, \delta = 0$.

$$K_e\begin{bmatrix} f_i' \\ \theta_i \\ f_j' \\ \theta_j \end{bmatrix} = F_e \quad (11)$$

The above system is solved for f' and θ distributions.

4. Code Validation

Table 1 shows the cade validation results. The obtained results are in good agreement with the existing results.

M	Present results	Noreen Sher et al. [2]
0	1.0015	1
0.5	-1.118028	-1.118039
1	-1.414290	-1.414211
5	-2.449460	-2.449491
10	-3.316619	-3.31663

5. Results and Discussion

The impact of these variables on dimensionless velocity and temperature profiles was determined using the numerical method described above for many relevant parameter values, including material parameters (ξ) and(δ), Prandtl number (Pr), Electric parameter($E1$), Magnetic parameter (M), and Eckert number (Ec).The computed outcomes are shown in figures. (2) - (9).

n temperature profile. As ξ augments the temperature profiles gets enhanced. Fig. 3(a)

depicts the impact of δ on the velocity field. An increment in δ leads to a diminishment in fluid velocity. As fluid parameter enhances the flow resistance improves so it reduces the velocity profiles. Temperature profiles exhibit a similar pattern of behaviour, as shown in Fig 3. (b). The impact of *Pr* on fluid velocity is very low as depicted in Fig. 4(a). It is evident from Fig. 4(b) as *Pr* augments the temperature profiles gets magnified in the presence of exponential heat source. Physically this means momentum diffusivity dominates the thermal diffusivity. It is evident from Fig. 5(a) an enhancement in *E1* causes an increment in velocity. As *E1* improves it augments the thickness of momentum boundary layer, so the velocity boosts up. Fig. 5(b) displays the impact of *E1* on the field of temperature. The large values of *E1* makes the temperature increase.

The impact of a magnetic parameter on velocity distribution is seen in Fig. 6(a). With an increase in the magnetic field, the boundary layer's thickness and velocity are both significantly reduced. This is attributed to the fact that the Lorentz force creates a resistance in opposite direction of the fluid flow. The effect of *M* on the temperature distribution is depicted in Fig. 6(b). An increase in *M* values is associated with a decrease in temperature. Fig. 7(a) manifests the pictorial description of velocity profile with the escalating values of *Ec*. As *Ec* improves a diminution in velocity is noticed. It is evident from Fig. 7(b) that an increment in temperature owing to an enhancement in the values of *Ec*. The physical explanation for this is that greater heat is produced due to the drag force between the fluid particles.

Fig. 8(a) is captured to analyse the effect of exponential heat source parameter Q_e on temperature distribution. It is noted that the velocity of the fluid decline for large values of Q_e. Fig. 8(b) establishes the impact of Q_e on temperature profiles. It clear that an increase in the exponential heat source parameter causes more energy to be converted into liquid, which improves the thermal boundary layer thickness and temperature profiles. Fig. 9(a) illustrates the fluid velocity is less influenced by Biot number. A drawing of Fig. 9(b) shows how *Bi* affects the temperature profile. It appears that as *Bi* improves, the temperature increases quickly close to the borders.

Figure 10 depicts the ANN configuration model. $\xi, \delta, Pr, E1, M, Ec, Qe,\ Bi\ and\ \eta$ are the input parameters, whereas the $f'and\ \theta$ are the output parameters. The available data set is separated into two datasets while constructing an artificial neural network model. The first dataset 20% is used to train the ANN model, and the second dataset 80% is used to validate it. The predicted outcomes of the ANN model are compared to the remaining data. The suggested technique employs LMB, SCGB, BRB, and RB, four different forms of back propagation algorithms.

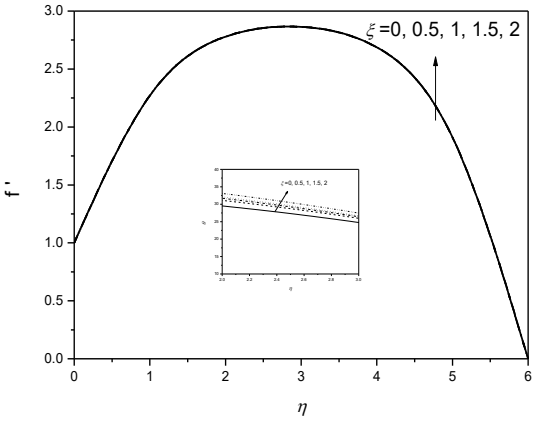

Fig.2(a). Variation of ξ on velocity profile

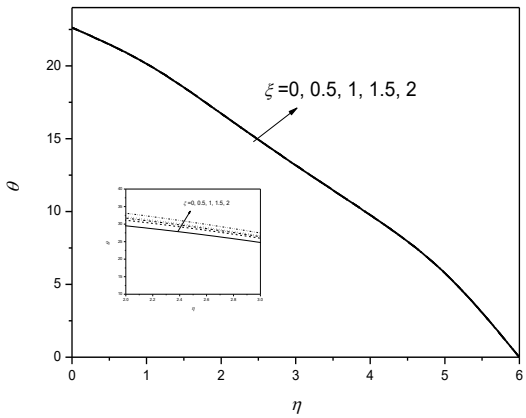

Fig.2(b). Variation of ξ on temperature profile

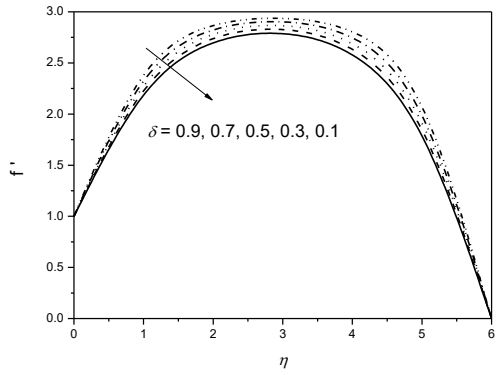

Fig.3(a). Variation of δ on velocity profile

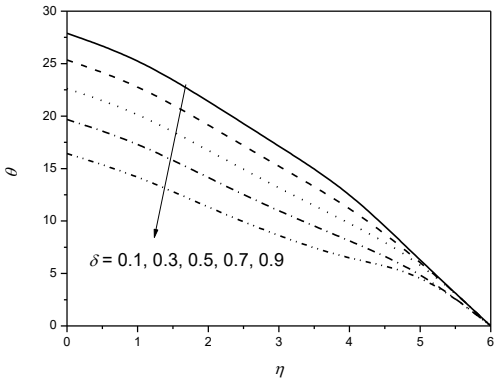

Fig.3(b). Variation of δ on velocity profile

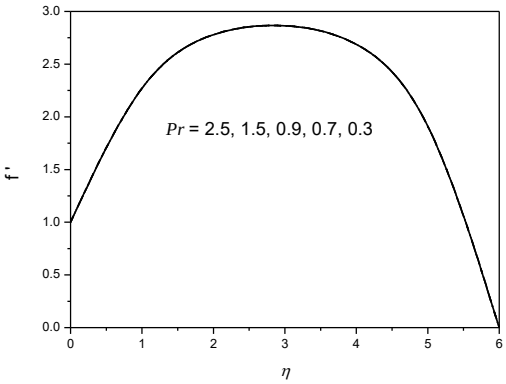

Fig.4(a). Variation of *Pr* on velocity profile

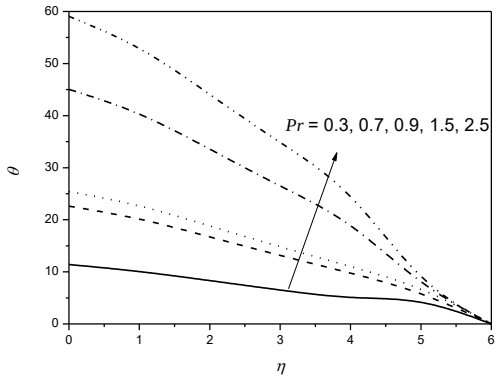

Fig.4(b). Variation of *Pr* on velocity profile

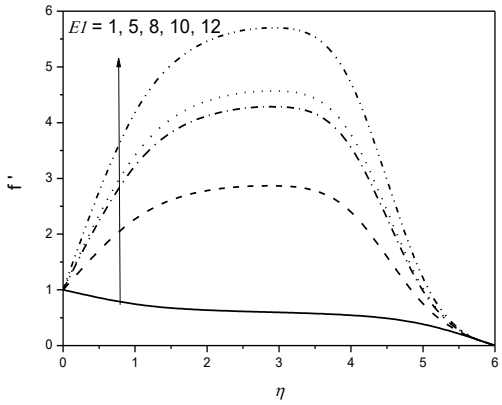

Fig.5(a). Variation of *E1* on velocity profile

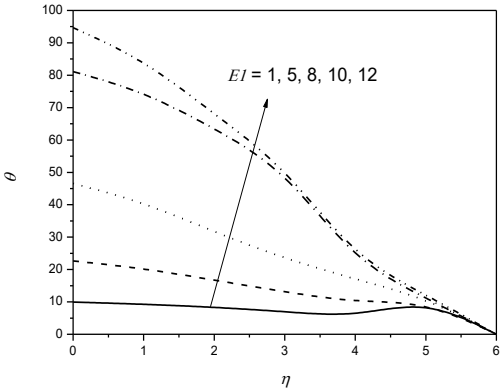

Fig.5(b).Variation of *E1* on temperature profile

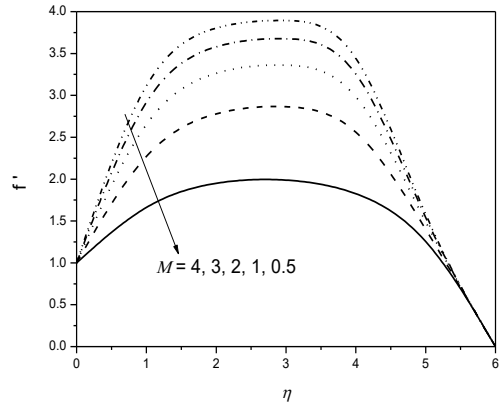

Fig.6(a). Variation of *M* on velocity profile

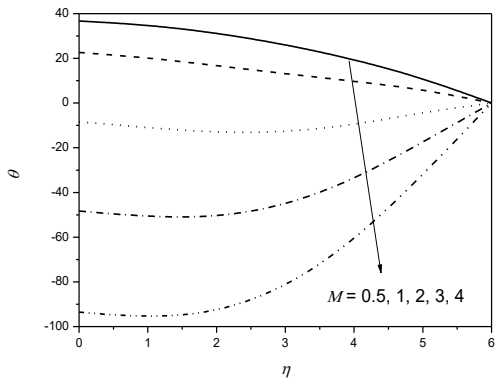

Fig.6(b). Variation of *M* on temperature profile

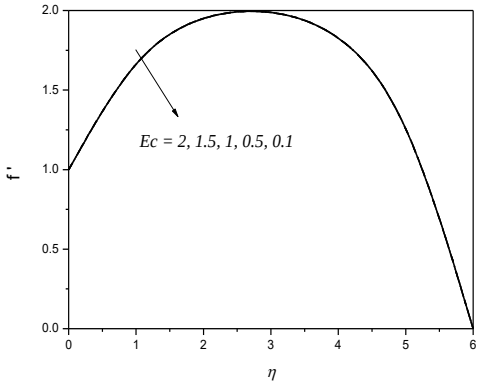

Fig.7(a). Variation of *Ec* on velocity profile

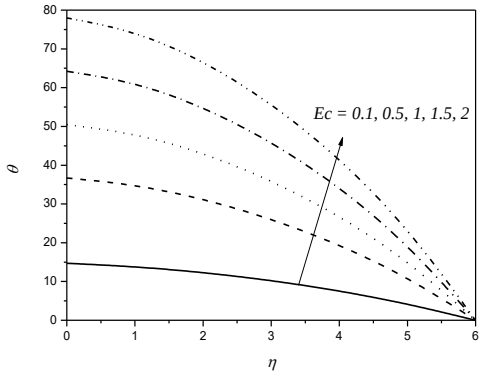

Fig.7(b). Variation of *Ec* on temperature profile

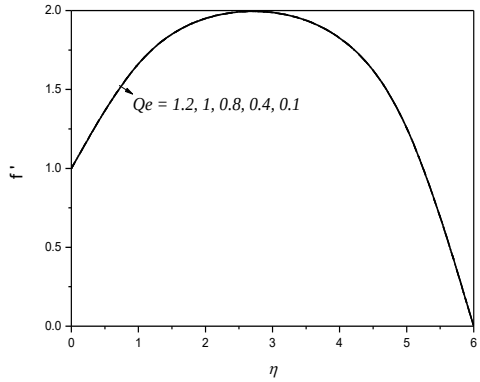

Fig.8(a). Variation of *Qe* on velocity profile

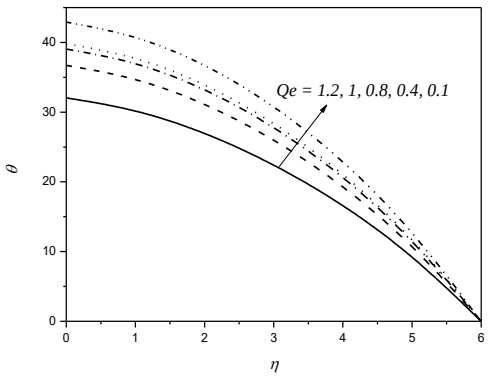

Fig.8(b). Variation of *Qe* on temperature profile

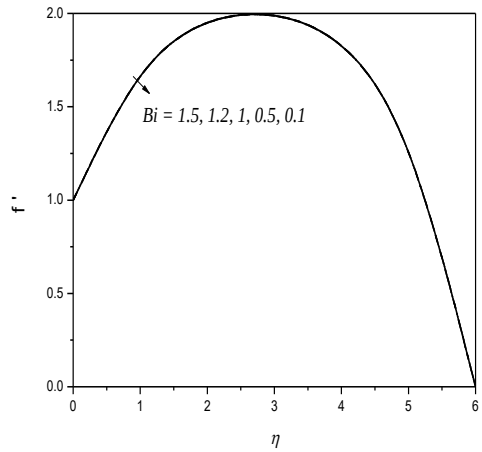

Fig.9(a) Variation of *Bi* on velocity profile

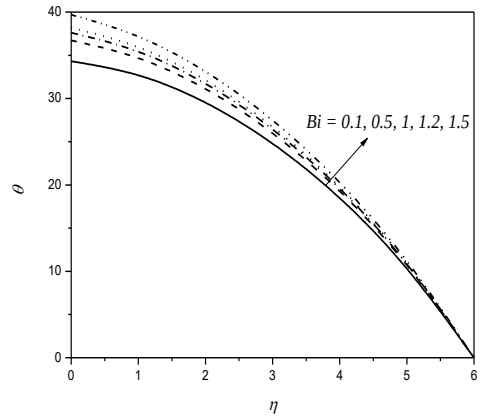

Fig.9(b).Variation of *Bi* on temperature profile

By changing the weights and biases, Fig. 10 attempts to reduce the error between expected output results and input data. Fig. 10 depicts the ANN model's architecture. The number of hidden layers and nodes in each layer are shown in this diagram. During training, a backward propagation algorithm is employed. In the hidden layer, all backward propagation techniques employ eight neurons. It uses a linear transfer function for the output layer and a tangent sigmoid transfer function (tansig) for the hidden layer.

An ideal ANN model is constructed using the dataset gained from the numerical inquiry to predict the velocity and temperature profiles. By changing the number of neurons in a hidden layer and planning the ANN's operation for each number, the best framework for the ANN can be discovered. As can be shown in Fig. 11, the findings of the optimal ANN are in a better agreement with the theoretical dataset and can predict the velocity

and temperature profiles more accurately than the correlation.

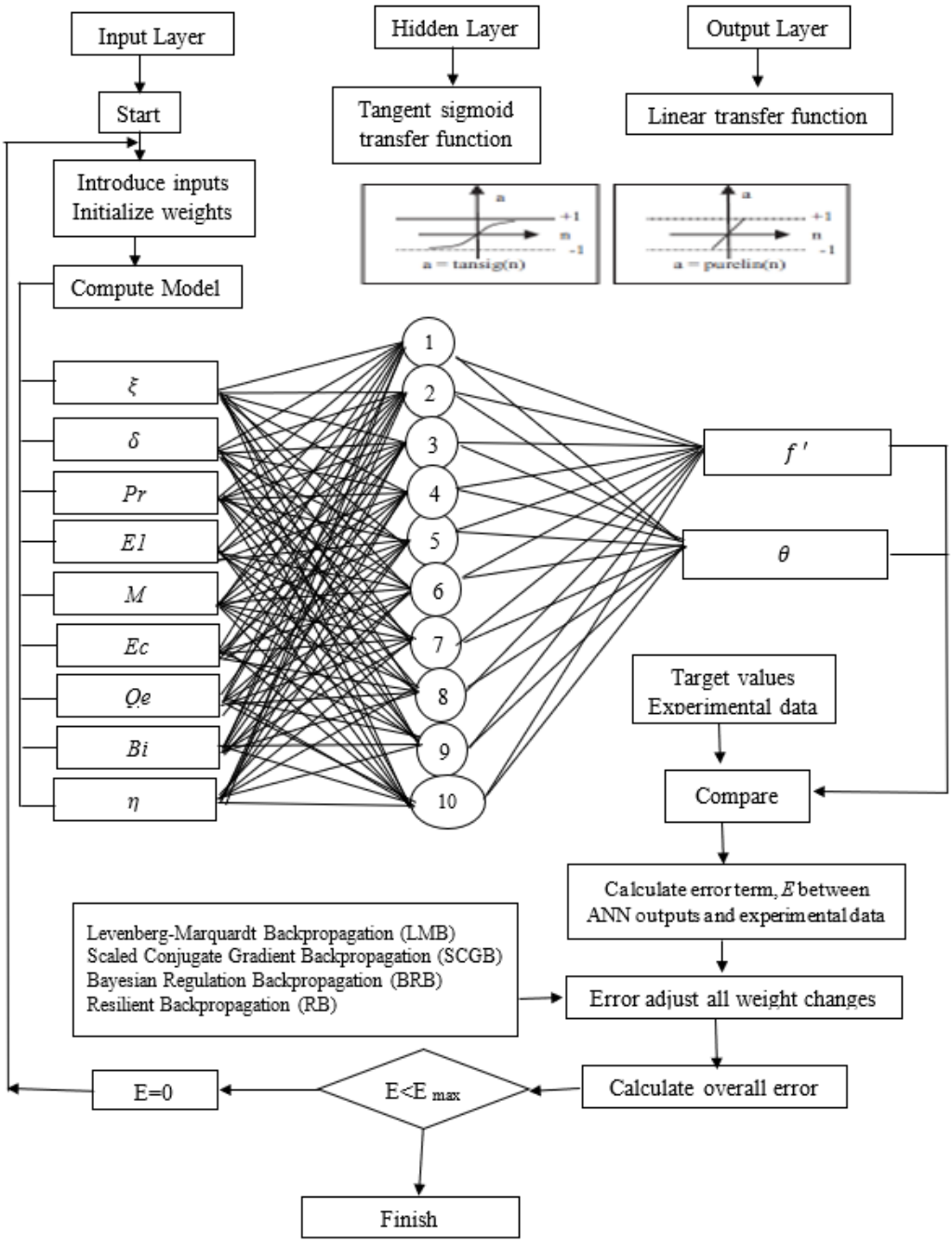

Fig.10. Proposed optimal architecture of the ANN model.

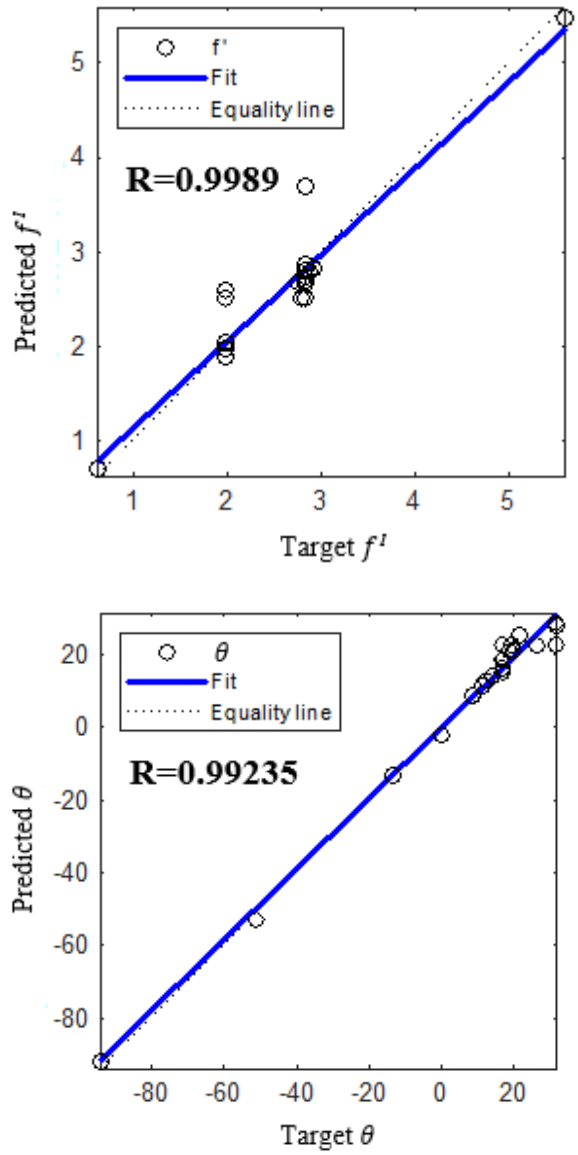

Fig. 11. Comparison between theoretical data and ANN outputs.

6. Concluding Remarks

In the current exploration an electro-osmotic flow of Eyring-Powell fluid over a stretching sheet in the presence of magnetic field, viscous dissipation and convective boundary conditions has been considered. The finite element method is implemented to discuss the nature of governing parameters. The developed ANN model is trained using CFD data to forecast the properties of heat transfer in the under-consideration channel with an accuracy of 99.89%. Graphical representations have been made of the influence of the relevant parameters on velocity and temperature profiles. Apropos to the above discussion, the following are the concluding points.

- Higher magnetic field shows diminishment in the velocity as well as temperature distributions.
- Assuming greater values for ξ, the temperature profiles get reduced and the velocity gets enhanced.
- As *Ec* improves, velocity of fluid decline and temperature will incline.
- Temperature and velocity profiles are both enhanced when *E1* is increased.

References

[1] R.E. Powell, H. Eyring, Mechanisms for the relaxation theory of viscosity [2], Nature. 154 (1944) 427–428. https://doi.org/10.1038/154427a0.

[2] N. Sher Akbar, A. Ebaid, Z.H. Khan, Numerical analysis of magnetic field effects on Eyring-Powell fluid flow towards a stretching sheet, J. Magn. Magn. Mater. 382 (2015) 355–358. https://doi.org/10.1016/j.jmmm.2015.01.088.

[3] S. Hina, MHD peristaltic transport of Eyring-Powell fluid with heat/mass transfer, wall properties and slip conditions, J. Magn. Magn. Mater. 404 (2016) 148–158. https://doi.org/10.1016/j.jmmm.2015.11.059.

[4] T. Hayat, M.I. Khan, M. Waqas, A. Alsaedi, Effectiveness of magnetic nanoparticles in radiative flow of Eyring-Powell fluid, J. Mol. Liq. 231 (2017) 126–133. https://doi.org/10.1016/j.molliq.2017.01.076.

[5] C.S. Reddy, N. Kishan, M. Madhu, Finite Element Analysis of Eyring–Powell Nanofluid Over an Exponential Stretching Sheet, Int. J. Appl. Comput. Math. 4 (2018) 1–13. https://doi.org/10.1007/s40819-017-0438-x.

[6] M. Gholinia, K. Hosseinzadeh, H. Mehrzadi, D.D. Ganji, A.A. Ranjbar, Investigation of MHD Eyring-Powell fluid flow over a rotating disk under effect of homogeneous-heterogeneous reactions, Case Stud. Therm. Eng. 13 (2019) 100356. https://doi.org/10.1016/j.csite.2018.11.007.

[7] A. Jafarimoghaddam, On the Homotopy Analysis Method (HAM) and Homotopy Perturbation Method (HPM) for a nonlinearly stretching sheet flow of Eyring-Powell fluids, Eng. Sci. Technol. an Int. J. 22 (2019) 439–451. https://doi.org/10.1016/j.jestch.2018.11.001.

[8] A.K. Ray, B. Vasu, P.V.S.N. Murthy, R.S.R.

*Corresponding e-mail: *nagabhushanamk.rvitm@rvei.edu.in* (Nagabhushana Pulla)

Gorla, Non-similar Solution of Eyring–Powell Fluid Flow and Heat Transfer with Convective Boundary Condition: Homotopy Analysis Method, Int. J. Appl. Comput. Math. 6 (2020). https://doi.org/10.1007/s40819-019-0765-1.

[9] M. Waqas, S. Jabeen, T. Hayat, S.A. Shehzad, A. Alsaedi, Numerical simulation for nonlinear radiated Eyring-Powell nanofluid considering magnetic dipole and activation energy, Int. Commun. Heat Mass Transf. 112 (2020) 104401. https://doi.org/10.1016/j.icheatmasstransfer.2019.104401.

[10] A. Riaz, Thermal analysis of an Eyring–Powell fluid peristaltic transport in a rectangular duct with mass transfer, J. Therm. Anal. Calorim. 143 (2021) 2329–2341. https://doi.org/10.1007/s10973-020-09723-7.

[11] Z. Nisar, T. Hayat, A. Alsaedi, B. Ahmad, Wall properties and convective conditions in MHD radiative peristalsis flow of Eyring–Powell nanofluid, J. Therm. Anal. Calorim. 144 (2021) 1199–1208. https://doi.org/10.1007/s10973-020-09576-0.

[12] F. Mabood, W. Farooq, A. Abbasi, Entropy generation analysis in the electro-osmosis-modulated peristaltic flow of Eyring–Powell fluid, J. Therm. Anal. Calorim. 147 (2022) 3815–3830. https://doi.org/10.1007/s10973-021-10736-z.

[13] A.S. Kotnurkar, S. Giddaiah, Bioconvection peristaltic flow of nano Eyring–Powell fluid containing gyrotactic microorganism, SN Appl. Sci. 1 (2019). https://doi.org/10.1007/s42452-019-1281-y.

[14] M.Z. Salleh, R. Nazar, I. Pop, Boundary layer flow and heat transfer over a stretching sheet with Newtonian heating, J. Taiwan Inst. Chem. Eng. 41 (2010) 651–655. https://doi.org/10.1016/j.jtice.2010.01.013.

[15] O. D, Makinde, Similarity solution for natural convection from a moving vertical plate with internal heat generation and a convective boundary condition. Thermal science, 15, (2011) 137-143. https://doi.org/10.1515/phys-2022-0228.

[16] Y. Khan, Q. Wu, N. Faraz, A. Yildirim, The effects of variable viscosity and thermal conductivity on a thin film flow over a shrinking/stretching sheet, Comput. Math. with Appl. 61 (2011) 3391–3399. https://doi.org/10.1016/j.camwa.2011.04.053.

[17] M. Subhas Abel, J. V. Tawade, M.M. Nandeppanavar, MHD flow and heat transfer for the upper-convected Maxwell fluid over a stretching sheet, Meccanica. 47 (2012) 385–393. https://doi.org/10.1007/s11012-011-9448-7.

[18] L. Zheng, C. Zhang, X. Zhang, J. Zhang, Flow and radiation heat transfer of a nanofluid over a stretching sheet with velocity slip and temperature jump in porous medium, J. Franklin Inst. 350 (2013) 990–1007. https://doi.org/10.1016/j.jfranklin.2013.01.022.

[19] M.M. Rashidi, N. Vishnu Ganesh, A.K. Abdul Hakeem, B. Ganga, Buoyancy effect on MHD flow of nanofluid over a stretching sheet in the presence of thermal radiation, J. Mol. Liq. 198 (2014) 234–238. https://doi.org/10.1016/j.molliq.2014.06.037.

[20] S. Das, R. N. Jana, and O. D. Makinde, MHD boundary layer slip flow and heat transfer of nanofluid past a vertical stretching sheet with non-uniform heat generation/ absorption. International Journal of Nanoscience, 13(03), (2014), 1450019. https://doi.org/10.1142/S0219581X14500197.

[21] M. Turkyilmazoglu, Flow of a micropolar fluid due to a porous stretching sheet and heat transfer, Int. J. Non. Linear. Mech. 83 (2016) 59–64. https://doi.org/10.1016/j.ijnonlinmec.2016.04.004.

[22] M.M. Bhatti, M.M. Rashidi, Effects of thermo-diffusion and thermal radiation on Williamson nanofluid over a porous shrinking/stretching sheet, J. Mol. Liq. 221 (2016) 567–573. https://doi.org/10.1016/j.molliq.2016.05.049.

[23] M.K. Nayak, N.S. Akbar, V.S. Pandey, Z.H. Khan, D. Tripathi, 3D free convective MHD flow of nanofluid over permeable linear stretching sheet with thermal radiation, Powder Technol. 315 (2017) 205–215. https://doi.org/10.1016/j.powtec.2017.04.017.

[24] S. Gupta, D. Kumar, J. Singh, MHD mixed convective stagnation point flow and heat transfer of an incompressible nanofluid over an inclined stretching sheet with chemical reaction and radiation, Int. J. Heat Mass Transf. 118 (2018) 378–387. https://doi.org/10.1016/j.ijheatmasstransfer.2017.11.007.

[25] M. Umar, R. Akhtar, Z. Sabir, H.A. Wahab, Z. Zhiyu, A. Imran, M. Shoaib, M.A.Z. Raja, Numerical Treatment for the Three-Dimensional Eyring-Powell Fluid Flow over a Stretching Sheet with Velocity Slip and Activation Energy, Adv. Math. Phys. 2019 (2019). https://doi.org/10.1155/2019/9860471.

[26] T. Hayat, S. Qayyum, A. Alsaedi, B. Ahmad, Entropy generation minimization: Darcy-Forchheimer nanofluid flow due to curved stretching sheet with partial slip, Int. Commun.

Heat Mass Transf. 111 (2020) 104445. https://doi.org/10.1016/j.icheatmasstransfer.2019.104445.

[27] R. Naveen Kumar, A.M. Jyothi, H. Alhumade, R.J. Punith Gowda, M.M. Alam, I. Ahmad, M.R. Gorji, B.C. Prasannakumara, Impact of magnetic dipole on thermophoretic particle deposition in the flow of Maxwell fluid over a stretching sheet, J. Mol. Liq. 334 (2021) 116494. https://doi.org/10.1016/j.molliq.2021.116494.

[28] W. Jamshed, S. Uma Devi S, M. Goodarzi, M. Prakash, K. Sooppy Nisar, M. Zakarya, A.H. Abdel-Aty, Evaluating the unsteady Casson nanofluid over a stretching sheet with solar thermal radiation: An optimal case study, Case Stud. Therm. Eng. 26 (2021) 101160. https://doi.org/10.1016/j.csite.2021.101160.

[29] A.S. Warke, K. Ramesh, F. Mebarek-Oudina, A. Abidi, Numerical investigation of the stagnation point flow of radiative magnetomicropolar liquid past a heated porous stretching sheet, J. Therm. Anal. Calorim. 147 (2022) 6901–6912. https://doi.org/10.1007/s10973-021-10976-z.

[30] S. Nadeem, W. Fuzhang, F.M. Alharbi, F. Sajid, N. Abbas, A.S. El-Shafay, F.S. Al-Mubaddel, Numerical computations for Buongiorno nanofluid model on the boundary layer flow of viscoelastic fluid towards a nonlinear stretching sheet, Alexandria Eng. J. 61 (2022) 1769–1778. https://doi.org/10.1016/j.aej.2021.11.013.

[31] Dharmaiah, G., O. D. Makinde, and K. S. Balamurugan. "Influence of Magneto Hydro Dynamics (MHD) Nonlinear Radiation on Micropolar Nanofluid Flow Over a Stretching Surface: Revised Buongiorno's Nanofluid Model." Journal of Nanofluids 11, 6 (2022): 1009-1022. https://doi.org/10.1166/jon.2022.1890.

[32] Shuguang Li, Farhan Ali, A. Zaib, K. Loganathan, Sayed M. Eldin, and M. Ijaz Khan. "Bioconvection effect in the Carreau nanofluid with Cattaneo–Christov heat flux using stagnation point flow in the entropy generation: Micromachines level study." Open Physics 21, (2023): 20220228. https://doi.org/10.1515/phys-2022-0228.

[33] Saravana, R., R. Hemadri Reddy, K. V. Narasimha Murthy, and O. D. Makinde. "Thermal radiation and diffusion effects in MHD Williamson and Casson fluid flows past a slendering stretching surface." Heat Transfer 51, no. 4 (2022): 3187-3200. https://doi.org/10.1002/htj.22443

[34] Shuguang Li, M. Ijaz Khan, Faris Alzahrani, and Sayed M. Eldin. "Heat and mass transport analysis in radiative time dependent flow in the presence of Ohmic heating and chemical reaction, viscous dissipation: An entropy modeling." Case Studies in Thermal Engineering (2023): 102722. https://doi.org/10.1016/j.csite.2023.102722.

[35] Shuguang Li, V. Puneeth, A. M. Saeed, A. Singhal, Fuad AM Al-Yarimi, M. Ijaz Khan, and Sayed M. Eldin. "Analysis of the Thomson and Troian velocity slip for the flow of ternary nanofluid past a stretching sheet." Scientific Reports 13, (2023): 2340. https://doi.org/10.1038/s41598-023-29485-0

[36] S. Mishra, B. Mahanthesh, J. Mackolil, P.K. Pattnaik, Nonlinear radiation and cross-diffusion effects on the micropolar nanoliquid flow past a stretching sheet with an exponential heat source, Heat Transf. 50 (2021) 3530–3546. https://doi.org/10.1002/htj.22039.

[37] P. Ragupathi, S. Saranya, H.V.R. Mittal, Q.M. Al-Mdallal, Computational Study on Three-Dimensional Convective Casson Nanofluid Flow past a Stretching Sheet with Arrhenius Activation Energy and Exponential Heat Source Effects, Complexity. 2021 (2021). https://doi.org/10.1155/2021/5058751.

[38] N.N. Reddy, V.S. Rao, B.R. Reddy, Chemical reaction impact on MHD natural convection flow through porous medium past an exponentially stretching sheet in presence of heat source/sink and viscous dissipation, Case Stud. Therm. Eng. 25 (2021) 100879. https://doi.org/10.1016/j.csite.2021.100879.

[39] P. M. Krishna, N. Sandeep, R. P. Sharma, Computational analysis of plane and parabolic flow of MHD Carreau fluid with buoyancy and exponential heat source effects, Eur. Phys. J. Plus. 132 (2017). https://doi.org/10.1140/epjp/i2017-11469-9.

[40] V.F. Formalev, M. Kartashov, S.A. Kolesnik, Wave Heat Transfer in Anisotropic Half-Space under the Action of a Point Exponential-Type Heat Source Based on the Wave Parabolic-Type Equation, J. Eng. Phys. Thermophys. 95 (2022) 366–373. https://doi.org/10.1007/s10891-022-02490-2.

[41] I. Ullah, M. Alghamdi, W.F. Xia, S.I. Shah, H. Khan, Activation energy effect on the magnetized-nanofluid flow in a rotating system considering the exponential heat source, Int. Commun. Heat Mass Transf. 128 (2021) 105578. https://doi.org/10.1016/j.icheatmasstransfer.2021.105578.

[42] K N Seetharamu, V Leela, Nagabhushanam

Kotloni, Numerical investigation of heat transfer in a micro-porous-channel under variable wall heat flux and variable wall temperature boundary conditions using local thermal non-equilibrium model with internal heat generation, International Journal of Heat and Mass Transfer, 112 (2017), 201–215.

[43] R W Lewis, P Nithiarasu, K N Seetharamu, Fundamentals of Finite Element Method for Heat and Fluid Flow, John Wiley & Sons. Ltd., (2004).

[44] P Nithiarasu, R W Lewis, K N Seetharamu, Fundamentals of Finite Element Method for Heat and Mass Transfer, second Edition, John Wiley & Sons. Ltd., (2016).